AGU PUBLICATIONS

Geochemistry, Geophysics, Geosystems

RESEARCH ARTICLE
10.1002/2016GC006704

Geochemistry of Zr, Hf, and REE in a wide spectrum of Eh and water composition: The case of Dead Sea Fault system (Israel)

P. Censi[1], M. Raso[1], Y. Yechieli[2,3], H. Ginat[4], F. Saiano[5], P. Zuddas[6], L. Brusca[7], W. D'Alessandro[7], and C. Inguaggiato[1,6,7]

[1]Department of Earth and Marine Sciences, University of Palermo, Palermo, Italy, [2]Geological Survey of Israel, Jerusalem, Israel, [3]Department of Hydrology and Microbiology, Zuckerberg Institute for Water Research, Ben-Gurion University of the Negev, Be'er Sheva, Israel, [4]Dead Sea and Arava Science Centre, Hevel Eilot, Israel, [5]SAF Department, University of Palermo, Palermo, Italy, [6]Sorbonne Universités, UPMC Univ. Paris 06, CNRS, Institut des Sciences de la Terre de Paris, Paris, France, [7]Istituto Nazionale di Geofisica e Vulcanologia, Palermo, Italy

Abstract Along the Jordan Valley-Dead Sea Fault area several natural waters in springs, wells, and catchments occur. The chemical-physical characters of the studied waters allowed for the first time the investigation of the Zr and Hf geochemical behavior, apart from REE, extended to a wide range of Eh, temperature, salinity, and pH conditions. The results of this study indicate that the dissolved Zr and Hf distribution in natural waters is strongly influenced by redox conditions since these in turn drive the deposition of Fe-oxyhydroxides or pyrite. In oxidizing waters saturated or oversaturated in Fe-oxyhydroxides (Group 1), superchondritic Zr/Hf values are measured. On the contrary, in waters where Eh < 0 values occur (Group 2), chondritic Zr/Hf values are found. Superchondritic Zr/Hf values are produced by the preferential Hf scavenging onto Fe-oxyhydroxides that is inhibited under reducing conditions consistent with the water oversaturation relative to pyrite. Redox conditions also influence the amplitude of Ce and Eu anomalies. Oxidized Group-1 waters show negative Ce anomalies related to the oxidative Ce scavenging as CeO_2 onto Fe-oxyhydroxide. Reduced Group-2 waters show positive Eu anomaly values consistent with the larger Eu^{2+} concentration relative to Eu^{3+} in these waters suggested by model calculations. The higher stability of Eu^{2+} with respect to its trivalent neighbors along the REE series can explain the above mentioned positive Eu anomaly values. The middle-REE enrichment observed in shale-normalized REE patterns of studied waters can be ascribed to carbonate and/or gypsum dissolution.

Key Points:
- Zr-Hf fractionation in studied natural waters is mainly driven by the stability of Fe-oxyhydroxides
- The extent of Eu and Ce anomaly values is determined by redox conditions
- The weathering of evaporites influences the features of shale-normalized REE distribution

Supporting Information:
- Supporting Information S1
- Table S1
- Table S2
- Table S3
- Table S4

Correspondence to:
P. Censi,
paolo.censi@unipa.it

Citation:
Censi, P., M. Raso, Y. Yechieli, H. Ginat, F. Saiano, P. Zuddas, L. Brusca, W. D'Alessandro, and C. Inguaggiato (2017), Geochemistry of Zr, Hf, and REE in a wide spectrum of Eh and water composition: The case of Dead Sea Fault system (Israel), *Geochem. Geophys. Geosyst.*, *18*, 844–857, doi:10.1002/2016GC006704.

Received 2 NOV 2016
Accepted 31 JAN 2017
Accepted article online 7 FEB 2017
Published online 3 MAR 2017

1. Introduction

Over the last 30 years, several papers about the aqueous geochemistry of the REE (lanthanides plus yttrium) have been published, whereas limited investigations have been carried out about Zr and Hf geochemistry [*Bau and Dulski*, 1995, 1999; *Byrne and Sholkovitz*, 1996; *Bau et al*., 1998; *Takahashi et al*., 2002; *Censi et al*., 2007a, 2010; *Göb et al*., 2013; *Inguaggiato et al*., 2016b]. The study of Zr and Hf distributions in natural waters started about 20 years ago and was mainly focused on seawater [*McKelvey and Orians*, 1993, 1998; *Godfrey et al*., 1996, 2009; *Firdaus et al*., 2011; *Frank*, 2011], apart from some studies focused on the aqueous speciation of these elements [*Aja et al*., 1995; *Byrne*, 2002; *Pershina et al*., 2002].

Several studies demonstrated the ability of the REE to provide insights about water-rock interactions processes [*Bau*, 1996; *Wood*, 2003; *Censi et al*., 2007b, 2014; *Biddau et al*., 2009; *Inguaggiato et al*., 2015; *Varekamp*, 2015]. The distribution of REE, Zr and Hf in waters is ruled by metal ion-complexation, precipitation and/or dissolution of solid phases and adsorption onto the mineral surfaces [*Wood*, 2003; *Bau and Koschinsky*, 2006; *Censi et al*., 2014; *Inguaggiato et al*., 2015].

Y-Ho and Zr-Hf are characterized by similar ionic radius and same charge. The twin pairs behave coherently during high-temperature processes such as the solidification of melt, where the elemental behavior is ruled by ionic radius and charge [*Comin-Chiaramonti et al*., 1992, 2007; *Censi et al*., 1989; *Ruberti et al*., 2002]. Y/Ho and Zr/Hf values are quite constant and close to the chondritic values in magmatic rocks with $SiO_2\% < 70$ [*Bau*, 1996]. Studies of Zr-Hf and Y-Ho in seawater and authigenic solids show the fractionation of these pairs leading to Y/Ho and Zr/Hf values far from the chondritic [*Censi et al*., 2014, 2015; *Schmidt et al*., 2014,

and references therein]. As a consequence, Zr/Hf values in open ocean water are larger than values recognized in coastal systems where the dissolution of lithogenic materials influences the Zr/Hf signature [*Godfrey et al*., 1996, 2009; *Firdaus et al*., 2011]. Hence, concentrations of dissolved Zr, Hf, and REE in natural waters depends on the weathering and nature of the source materials and the elemental removal during the formation of authigenic, biogenic and inorganic solids as carbonates, SiO_2, Fe-oxyhydroxides, and Mn-oxyhydroxides [*Inguaggiato et al*., 2016a].

In this study, the geochemistry of Zr, Hf, and REE was investigated in continental waters along the Dead Sea Fault (Israel). This study area was chosen for the large variability in chemical-physical conditions and chemical compositions of the waters, in order to evaluate the different behavior of REE, Zr, and Hf possibly induced by changes of pH, Eh, ionic strength, and precipitation of authigenic minerals.

2. Geological Setting

The investigated area of the Dead Sea Transform (DST) is the northern part of the Syrian-Red Sea-East-Africa transform [*Garfunkel*, 1981]. The transform itself is the boundary between, the Arabian Plate in the east and the African Plate in the west. The crustal part consists of an old crystalline basement (more than 580 Ma old) underlying thick sedimentary rock sequences [*Ginzburg and Gvirtzman*, 1979; *Rybakov and Segev*, 2004]. Only in the southernmost area, close to Eilat, does the crystalline basement occur [*Lustrino and Wilson*, 2007]. The sedimentary sequences consist of carbonates, sandstones, clays, and evaporites in the northern part of the investigated area, close to lake Kinneret [*Zak*, 1967; *Weinstein et al*., 2000].

The whole geological structure can be divided into three main areas. The northern areas built of Miocene-Quaternary volcanism and continental sediments belonging to the Tiberias Group in the eastern part of the investigated area (near the Golan Heights) while the western part (adjacent to the Galilee Mountains) is made mostly of carbonate sequences of Judea, Mt. Scopus and Avdat groups. The central part of the studied area is from the Lake Kinneret to the southern Dead Sea. It is limited in the west by the eastern Judea and Samaria Mountains whereas the transform faults represent the eastern limit of the escarpment. The southernmost part of this area is composed of evaporitic and alluvium sequences belonging to the Dead Sea Group [*Mechie et al*., 2013]. The third part of the studied area, extending between the Dead Sea and the Gulf of Eilat, is mostly a low area filled by thick alluvium deposits. This southern part is limited between Precambrian crystalline rocks covered by Precambrian magmatic and metamorphic rocks and sandstones both forming the Edom mountains at East and the carbonate sequences of the Judea Group outcropping in the Negev area in the west. Several geological information about the Geology of Israel occurs can be recognized in several studies [*Sneh et al*., 1998; *Gur et al*., 2003; *Greitzer and Levitte*, 2000; *Levitte and Greitzer*, 2005; *Reznikov et al*., 2004, and references therein].

3. Materials and Methods

Samples of several natural waters were collected for this study along the Lake Kinneret-Jordan Valley-Dead Sea rift area. Sampling sites are located at Banias springs, in the Golan Heights, Hamei Teveria spring along the northern and western shores of the lake Kinneret, the shallow water of lake Kinneret, Qedem springs, and Ein Gedi thermal water collected from the well located in the local spas along the western shore of Dead Sea. Yishai spring water was collected in a little pool close to the Dead Sea shoreline between Ein Gedi and Qedem. Hamei Yoav and Hamei Gaash waters come from the western plan of Israel along the Mediterranean coast. Qetura and Ya'Alon are samples coming from the southern Israel and were collected from wells. Sample collection was carried out during May 2013, March 2014, and May 2015. The location of collection sites is reported in Figure 1.

Eh, pH, temperature, and conductivity of the studied waters were measured directly in the field with an ORION 250+ m. Eh measurement was carried out with an Eh oxytrode Pt probe (Hamilton^{TM}) using a reference standard solution buffer at 0.475 $\pm$ 0.005 V. Accuracy of determinations was $\pm$0.01 V for Eh, $\pm$0.1 for pH, $\pm$0.1°C for temperature, and 1% for EC. The major anions were analyzed by Dionex ICS 1100 chromatograph on filtered and acidified (HNO_3) samples with a Dionex CS-12A column for cations and on filtered and acidified (HNO_3) samples with a Dionex AS14A column for anions. Alkalinity was determined in the field by titration with HCl 0.1 *M*. Thereafter, 1 L of water was collected at each sampling site, immediately filtered

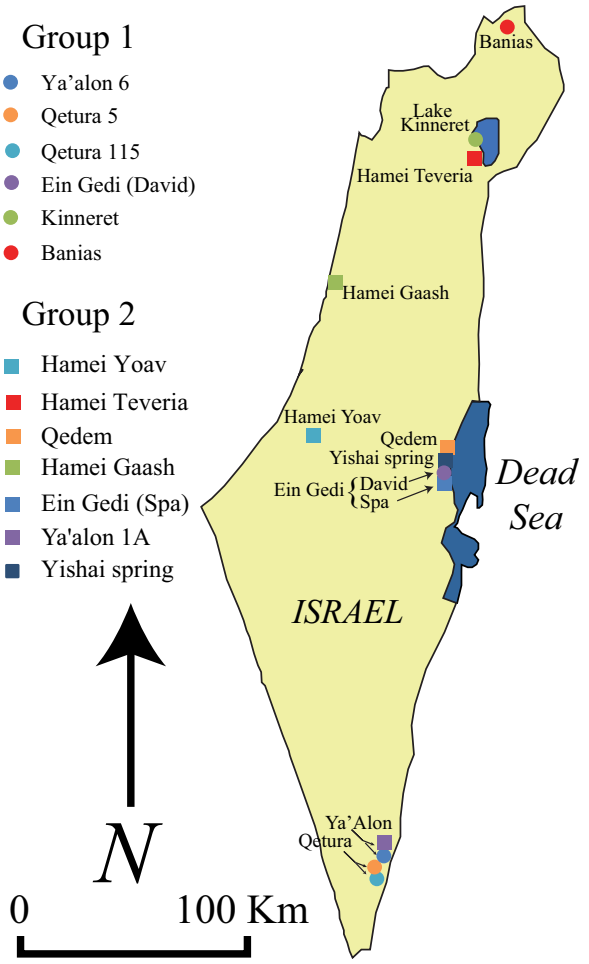

Figure 1. Location of sampling sites. Circles represent Group-1 waters, whereas squares identify Group-2 waters.

(0.45 μm filter membrane), acidified with 1% HNO_3 ultrapure solution to attain pH ≈ 2 and then stored in previous cleaned polyethylene bottles. In order to separate studied elements from the remaining solution in both fractions, a NH_4OH (25%) solution was added to attain pH = 8 and then an excess of $FeCl_3$ (1%) solution was added to induce the precipitation of solid $Fe(OH)_3$. REE, Zr, and Hf are scavenged onto the surface of the crystallizing $Fe(OH)_3$ and can be separated from the remaining liquid. In order to be sure that the crystallization of Fe-hydroxide is complete, the solution was left in a closed flask for 48 h and then Fe hydroxide collected onto a membrane filter (Millipore™ manifold filter diameter 47 mm, pore size 0.45μm). Fe hydroxide was dissolved in HCl 6 *M*. The obtained solution was diluted 1:6 and analyzed in quadrupole-ICP-MS (Agilent 7500cc) with an external calibration procedure.

All chemicals used during laboratory manipulations were of ultrapure grade. Ultra-pure water (resistivity of 18.2 Ω cm) was obtained by an EASY pure II purification system (Thermo, Italy). Nitric acid 65% (w/w), ammonia solution, and hydrochloric acid were purchased from VWR International. Working standard solutions for each element (Zr, Y, La, Ce, Pr, Nd, Sm, Eu, Gd, Tb, Dy, Ho, Er, Tm, Yb, Lu, and Hf) were prepared on a daily basis by stepwise dilution of the multielement stock standard solution DBH, Merck, or CPI International (1000 ± 5 μg mL^{-1}) in a HCl 1 *M* medium.

In order to assess possible interferences of BaO^+ on Eu^+ mass, the entire calibration procedure was performed with calibration solutions having a Ba/Eu weight ratio of 10,000. Furthermore, during the entire analytical session in order to evaluate the accuracy of analysis, certified reference waters (Spectrapure Standards, Norway) containing both elements at two different concentrations: 0.5 ppb of Eu and 50 ppb of Ba in SPSSW1, 2.5 ppb of Eu and 250 ppb of Ba in SPSSW2 were repeatedly analyzed and the results were always within ±10% for both elements.

All labware was in polyethylene, polypropylene, or in Teflon and the calibration of all volumetric equipment was verified. A calibrated E42-B balance (Gibertini, Italy) was used to weigh all samples and standards. pH measurements were carried out with HI 991300 pH-meter (Hanna Instruments, Italy).

The assessment of the analytical precision of REE, Zr, and Hf was hard to carry out since, to the author's knowledge, aqueous standard reference materials with REE, Zr, and Hf concentrations referenced or simply indicated are not known. Hence, as previously carried out by *Raso et al.* [2013], three aliquots (1 L each) of NASS-6 (distributed by National Research Council of Canada) were treated as water samples according to the above mentioned procedure and the obtained concentrations compared with those previously reported in literature (see supporting information Table S1).

Dissolved speciation of investigated elements and saturation indexes of minerals have been calculated with the PHREEQC software package (version 3.0.6) [*Parkhurst and Appelo*, [2010]. This choice was carried out in order to get only qualitative information about suitable REE, Zr, and Hf dissolved speciation in so extreme environments. These calculations have been performed using compilations of stability constants of REE

complexes occurring in LLNL database, integrated by more recent thermodynamic values [*Millero*, 1992; *Lee and Byrne*, 1992; *Klungness and Byrne*, 2000; *Luo and Byrne*, 2000, 2001, 2004; *Schijf and Byrne*, 2004] as previously carried out in *Johannesson et al.* [2004], *Tang and Johannesson* [2006], and *Leybourne et al.* [2006]. Aqueous Zr and Hf speciation was not assessed with the PHREEQC software since it is always the same in a wide range of physical-chemical conditions and described in depth in previous researches [*Aja et al.*, 1995; *Byrne*, 2002].

Scanning Electron Microscopic (SEM) observations and EDS spectra were carried out on suspended particulate matter (SPM) collected in studied waters after filtration. SPM were gently dried under vacuum, mounted on aluminum stubs and gold coated. SEM observations were carried out using a LEO 440 SEM equipped with an EDS system OXFORD ISIS Link and Si (Li) PENTAFET detector that was used to provide EDS spectra.

4. Results

4.1. General Aspects

The chemical-physical parameters and major elements concentrations of the studied waters are reported in supporting information Table S2. Water temperature ranges between 14.6 and 57.2°C and pH values range from 5.4 to 8.5. Waters with lower pH values have higher amount of CO_2 dissolved in waters [*Inguaggiato et al.*, 2016b]. The total dissolved salts (TDS) and the Eh values cover a wide range from 0.3 to 193.5 g L^{-1} and −0.4 to 0.26 V, respectively. Sample waters are characterized by a wide spectrum of major elements composition due to the mixing between meteoric water and ancient brines interacting with local rocks, as found by previous studies [*Moller et al.*, 2007]. The anion triangular plot shows water compositions falling along the imaginary line jointing the Cl and HCO_3 vertices, probably representing the mixing between brines and meteoric waters interacting with carbonate rocks (Figure 2a).

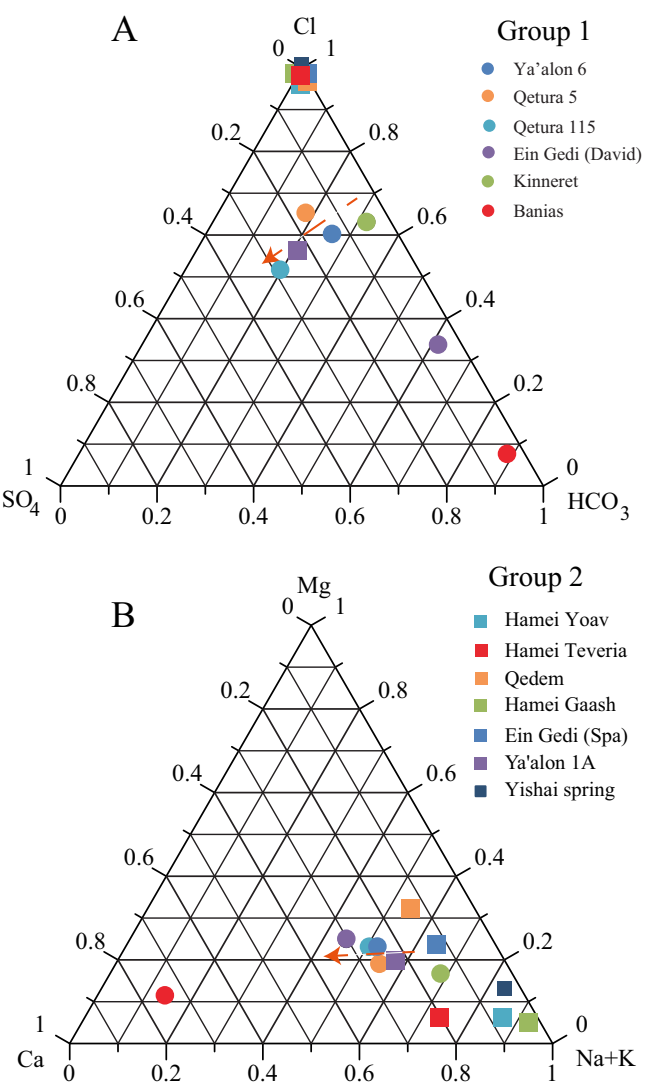

Figure 2. (a) Triangular plot of major anions dissolved in water. The red arrow indicates SO_4 enrichments probably due to the gypsum dissolution. (b) Triangular plot of major cation dissolved in water. The red arrow indicates Ca enrichments probably due to the gypsum dissolution.

A group of waters (Ya'alon 1a, Ya'alon 6, Qetura 5 e Qetura 115) is characterized by a relative enrichment in SO_4^{2-} compared to the other waters, showing in the triangular plot a deviation of the samples toward the SO_4 vertex (Figure 2a). The cation triangular plot shows both waters falling close to the Na-K corner with a slight dispersion toward both the Ca and Mg corners (Figure 2b). The water with Ca dominated composition is Banias, whereas the waters with relative high Ca contents are the samples characterized by relative high SO_4 contents. The enrichment of Ca^{2+} and SO_4^{2-} is explained by the dissolution of gypsum, whereas the waters with high Na-Cl contents are ancient brines or meteoric water dissolving halite [*Moller et al.*, 2007].

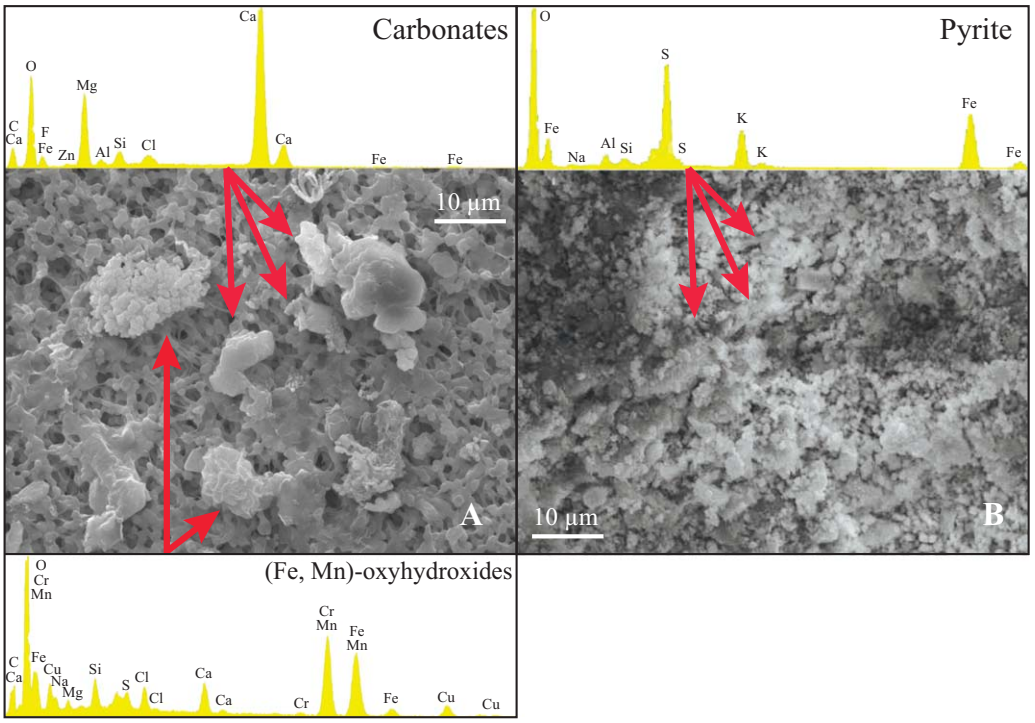

Figure 3. Carbonate (dolomite) crystal aggregates, Fe-, Mn-oxyhydroxides, and Pyrite microcrysts in SPM collected from (a) Group-1 and (b) Group-2 waters, respectively.

The waters were classified according to their Eh values and consequently to their saturation indexes with respect to Fe-bearing minerals and to Eh values (supporting information Table S3). Based on this approach, two different water groups were identified: Group 1 formed by waters from slightly undersaturated to oversaturated relative to Fe-oxyhydroxides with Eh values ranging between −0.1 and 0.26 V; Group 2 formed by pyrite oversaturated waters with Eh values lower than −0.25 V. Some Group-1 and Group-2 waters are saturated or oversaturated with respect to dolomite and calcite whereas the studied waters are always undersaturated with respect to gypsum and halite.

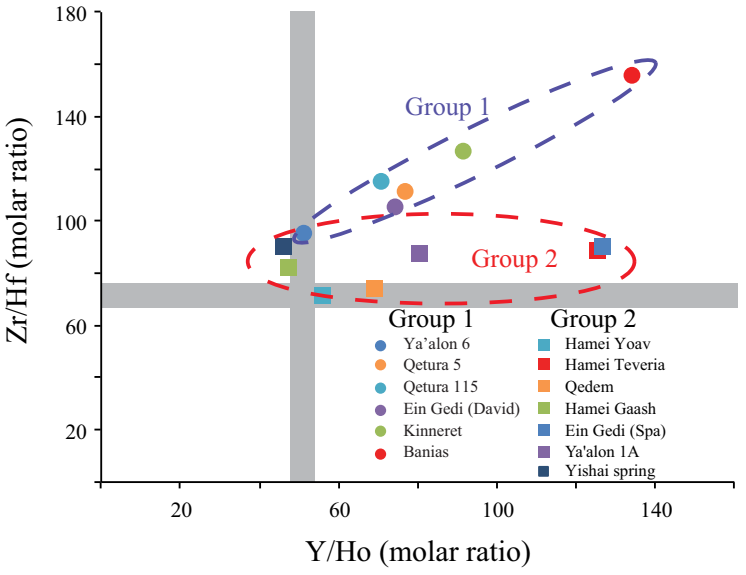

Figure 4. (a) Zr-Hf and (b) Y-Ho molar ratios. The grey bands indicate the chondritic Y/Ho and Zr/Hf ratio values according to *Jochum et al.* [1986]. Standard error is within the symbols.

Scanning electron microscopy (SEM) observations carried out on SPM from the studied waters show lithic fragments, crystals and apparently amorphous or cryptocrystalline materials. SEM-EDS analyses revealed Mn- and Fe-oxyhydroxides coupled with calcite and/or dolomite in Group 1 (Figure 3).

4.2. REE, Zr, and Hf

Zr and Hf concentrations range from 11 to 955 pmol L^{-1} and 0.3–10 pmol L^{-1}, respectively (supporting information Table S4). The amount of Y and Ho dissolved in waters ranges from 6.2 to 1066 pmol L^{-1} and

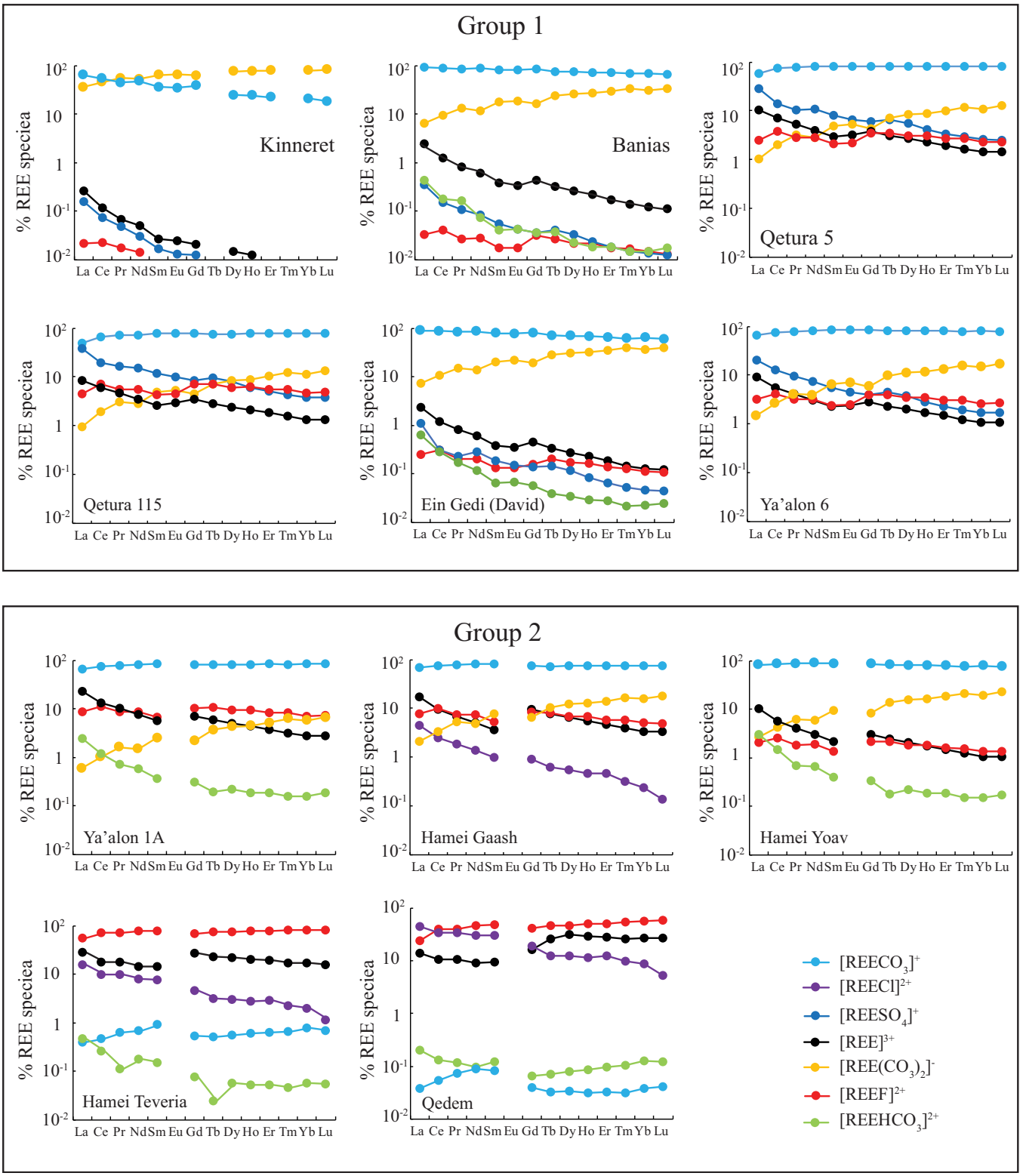

Figure 5. Relative abundances (percentage) of the REE complexes in some investigated waters. In highly saline waters at Yishai spring and Ein Gedi Spa, the calculation of REE speciation attained unreasonable results that are not included. In Group-2 waters (Eh ≤ -0.25 V), model calculations suggest Eu^{2+} as the most abundant Eu species. Since very little is known about the aqueous speciation of Eu(II) [see *Sverjensky*, 1984], Eu model calculations are not reported.

from 0.05 to 15.1, respectively. Zr/Hf and Y/Ho molar ratios change between 68.1–156 and 41.8–134.3, respectively, from close to chondritic (70.8 ± 5.6 and 51.2 ± 5, respectively) [*Jochum et al*., 1986] to superchondritic values. Figure 4 shows that Y/Ho and Zr/Hf ratios change simultaneously in Group 1 toward superchondritic values, whereas a different behavior was found in Group 2 with Zr/Hf ratios always close to chondritic values and Y/Ho ratios spanning from chondritic to superchondritic. REE speciation in Groups 1 and 2 shows REE-complexes dominated by carbonate and halide species (Figure 5).

As well as can be expected, the relative abundances of REE complexes is dominated by carbonate species in studied waters, apart from in Hammei Teveria e Qedem springs where chloride and fluoride complexes are the most abundant aqueous species. Moreover, Figure 5 suggests the significant contribution of aqueous REE complexes to the whole budget of these elements in dissolved phase. With any probability, this evidence is related to pH value recognized at Qedem (pH = 5.4) that is the lowest among those found in studied waters. The significant contribution of aquo-REE complexes at Qedem leads to a LREE (firstly La) enrichment in dissolved phase that is reflected by the highest La concentrations recognized both there and at Yishai spring among the studied waters. On the contrary, Zr and Hf speciation does not change for the range of pH values recognized in waters from Groups 1 and 2 [*Byrne*, 2002].

The total REE contents range from 19.1 to 2977.8 pmol L^{-1} (supporting information Table S4). Figure 6 shows the shale-normalized REE patterns, relative to PAAS (Post Archean Australian Shale) [*Taylor and McLennan*, 1995]. Group-1 waters show patterns slightly increasing along the REE series and medium REE (MREE) enriched at Qetura 5, Qetura 115, Ya'alon 6 and in Lake Kinneret. Moreover, negative Ce anomalies are found in almost all waters belonging to Group 1. Group-2 waters show shale-like patterns with slight MREE enrichments centerd on Gd or Eu whereas there is a strong MREE enrichment and lack of Eu anomalies in Ya'alon 1a water. Moreover, Group 2 is characterized by strong Eu anomalies and no Ce anomalies. Ya'alon 6 water shows REE characters intermediate between those of Group-1 and Group-2 waters. In fact, it shows the MREE enrichment typical of the Group-1 water but it is free from positive Ce anomaly

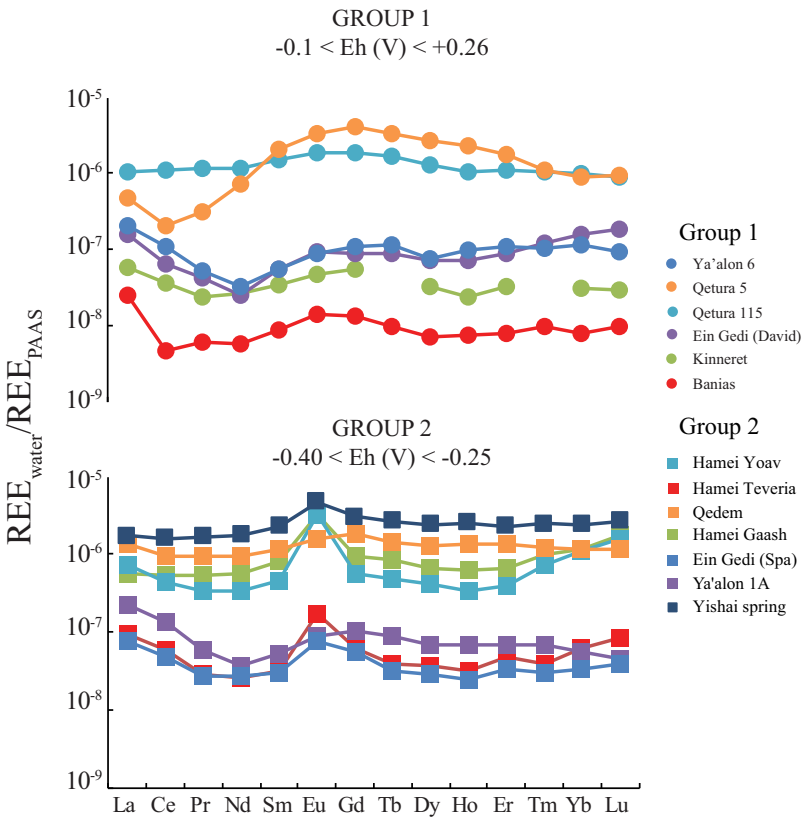

Figure 6. Shale-normalized REE patterns of the studied waters relative to PAAS [*Taylor and McLennan*, 1995]. Standard error is within the symbols.

(characteristic of Group-1 water) and Eu anomaly (characteristic of Group-2 water), probably as a consequence of the Eh value close to −0.1 V intermediate between the two groups.

5. Discussion

5.1. Zirconium and Hafnium

Previous studies carried out on natural waters from the Rift Valley-Dead Sea area [*Möller et al*., 2003; *Moller et al*., 2007; *Siebert et al*., 2012] did not take in account the Zr and Hf behavior and considered the dissolved REE distribution as mainly related to the effects of water-rock interactions in different aquifers. The latter processes were considered responsible for a wide spectrum of dissolved compositions under the different thermochemical conditions occurring in the waters.

Figure 7 shows that Zr/Hf molar ratios increase as Eh values increase. Group-2 waters have Zr/Hf molar ratios quite constant clustered around the chondritic signature whereas Group-1 waters have Zr/Hf ratios directly related to Eh values starting from the chondritic signature. Considering that Zr and Hf are not redox sensitive elements and their dissolved speciation is not influenced by redox conditions [*Byrne*, 2002], the different Zr/Hf ratios found in Groups 1 and 2 can be related to the different affinity of Zr and Hf aqueous complexes toward solid surfaces. In a wide range of pH values, $(Zr(OH)_4)^0$ and $(Hf(OH)_5)^-$ are indicated as the most abundant aqueous species of Zr and Hf [*Aja et al*., 1995]. Their affinity toward solid surfaces was observed under different natural conditions [*Godfrey et al*., 1996; *Bau and Koschinsky*, 2006; *Lutfi Firdaus et al*., 2008; *Firdaus et al*., 2011; *Censi et al*., 2015]. It was related to the charge of the dissolved species in relation to the electrostatic surface charge of the sorbent according to a coulombic electrostatic model [*Koschinsky and Hein*, 2003, and references therein]. According to this model, some suitable sorbent species in studied waters can be considered the most abundant saturated and oversaturated minerals (Fe-oxyhydroxides, as goethite according to model calculations and pyrite or a pyrite precursor such as mackinawite in Group-1 and Group-2 waters, respectively). Figure 8 shows that Zr/Hf ratio is almost constant around the chondritic signature in Fe-oxyhydroxide undersaturated Group-2 waters whereas superchondritic values are recognized in oxidizing Fe-oxyhydroxide oversaturated Group-1 waters (Figure 8a). Again, the extent of

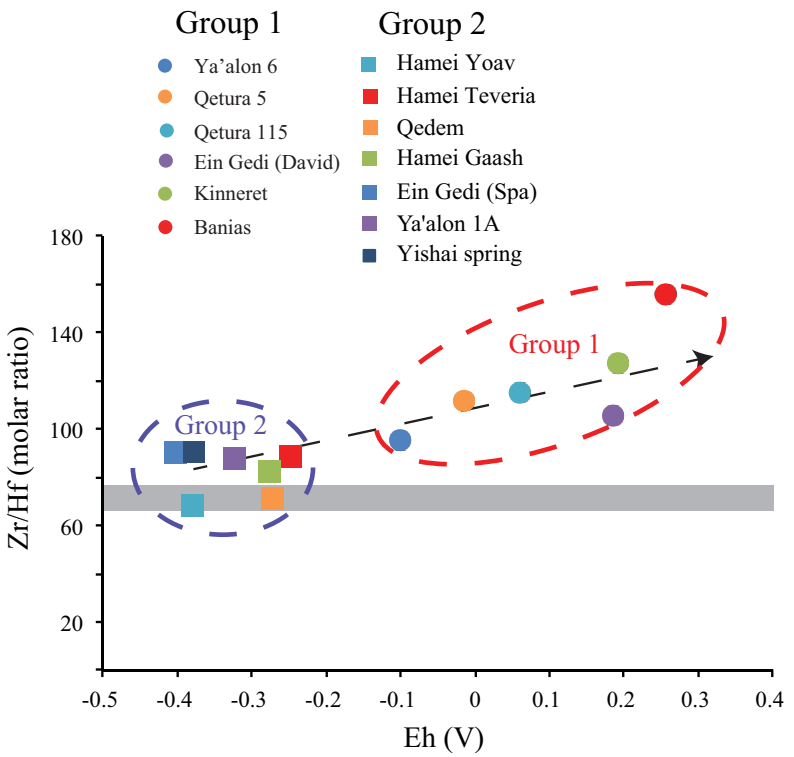

Figure 7. Zr/Hf molar ratios versus Eh values. The grey band indicates the chondritic Zr/Hf ratio values according to *Jochum et al*. [1986]. Standard error of Zr/Hf values is within the symbols.

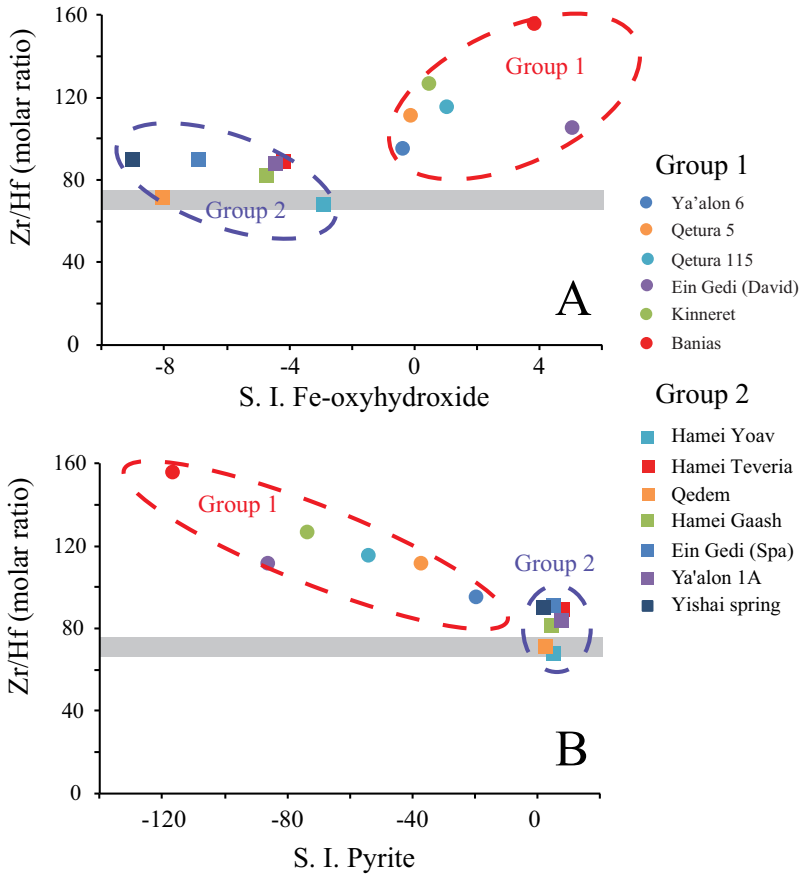

Figure 8. (a) Zr/Hf molar ratios versus saturation indexes of Fe-oxyhydroxides. (b) Zr/Hf molar ratios versus saturation indexes of pyrite. The grey bands indicate the chondritic Zr/Hf ratio values according to *Jochum et al.* [1986]. Standard error of Zr/Hf values is within the symbols.

superchondritic signature of Zr/Hf ratio progressively decreases relative to saturation index of pyrite in Group-1 waters closely attaining the chondritic value in pyrite-saturated Group-2 waters (Figure 8b). These evidences are consistent with the large capability of goethite surfaces to interact with dissolved acidic species that are directly bound with surface Fe atoms from acidic to circumneutral pH as those occurring in Group-1 waters [*Marsac et al.*, 2016]. On the other hand, a limited interaction of aqueous $(Zr(OH)_4)^0$ and $(Hf(OH)_5)^-$ complexes is expected onto pyrite surfaces where zeta potential is neutral or negative at pH $\geq$ 5.5 [*Vergouw et al.*, 1998; *Bulbul et al.*, 2016]. The latter indication is consistent with the limited Zr-Hf decoupling observed in Group-2 waters where Zr/Hf values are clustered closely to the chondritic signature.

5.2. Yttrium and Holmium

Differently from the Zr and Hf behavior during dissolved complexation, the Y and Ho dissolved species always show the same ionic charge if complexed with the same ligand. Therefore, the Y–Ho decoupling observed in almost all of the Group-1 and Group-2 waters (Figure 4) cannot be driven by electrostatic considerations, probably depending from the different covalent character of the dissolved Y and Ho complexes [*Bau*, 1996]. This suggestion is confirmed by the preferential Ho scavenging onto Fe-oxyhydroxide relative to Y [*Bau*, 1999]. Laboratory experiments on $CaCO_3$ crystallization (both calcite and aragonite) indicate the preferential incorporation of Ho into $CaCO_3$ relative to Y [*Qu et al.*, 2009]. These results were confirmed by *Tanaka et al.* [2004, 2008] recognizing a preferential Y enrichment relative to Ho in the dissolved phase during calcite crystallization that was interpreted as a Ho–CO_3 and Y–CO_3 bonding difference in carbonate minerals.

5.3. Rare Earths

Figure 5 shows that the most abundant REE species in Group 1 are $(REECO_3)^+$ and $(REE(CO_3)_2)^-$ complexes. The progressive increasing of the observed percentage $REE(CO_3)_2^-$ content from La to Lu agrees

with the growth of the stability constant of this complex along the REE series [*Millero*, 1992; *Luo and Byrne*, 2004].

The arrangement of Qetura 5, Qetura 115, Ya'alon 1A, and Ya'alon 6 waters in Figure 2 and their MREE enrichment reported in shale-normalized patterns (Figure 6) suggest that these waters experienced sulphate dissolution during groundwater circulations. This suggestion agrees with the lithology of their aquifers in the western side of the Arava graben, consisting of Lower Cretaceous sandstones with anhydrite cement or lenses [*Möller et al*., 2009, and references therein]. Sulphate minerals, mainly anhydrite and gypsum, often show normalized REE patterns characterized by MREE enriched irrespectively from their primary [*Bach et al*., 2003; *Playa et al*., 2007; *Schmidt et al*., 2014] or detritic nature [*Toulkeridis et al*., 1998].

Also the water from lake Kinneret shows similar MREE enrichment. But it cannot be originated from sulfate dissolution since the major ion composition of this water falls along the Cl^{-}-HCO_3^{-} and Mg^{2+}-$(Na^{+} + K^{+})$ sides in Figures 2a and 2b, respectively. Therefore, a further explanation of the MREE enrichment in the lake Kinneret water has to be found.

Usually, MREE enrichments in natural waters can be determined by the dissolution of MREE fractionating solids, as previously mentioned for gypsum. Some evidences of MREE enrichment in river waters are reported consequently to phosphate dissolution [*Hannigan and Sholkovitz*, 2001] or during the leaching of Fe-oxyhydroxides. But the former process leads to shale-normalized patterns where MREE enrichment is coupled with negative Ce anomaly values, whereas the formed even allows to positive Ce anomalies other than MREE enrichment since both Ce and MREE are enriched onto Fe-oxyhydroxides.

Recently, the recycling of organic products by bacteria in the Lake Kinneret was recognized as a key factor for influencing the nutrient supply to phytoplankton [*Li et al*., 2014], whereas these organisms are responsible of iron reduction from Fe(III) to Fe(II) in the water lake [*Shaked et al*., 2002]. Here iron is mainly provided both by Fe-rich particles and colloids coming from the Jordan river. These materials usually represent the main vehicle for the transport of REE and other trace elements in rivers where these metal ions are adsorbed onto the surface of Fe-rich products [*Sholkovitz*, 1995; *Hannigan and Sholkovitz*, 2001]. Since Fe-rich materials in rivers are enriched in MREE [*Bau*, 1999; *Ohta et al*., 2009], their mineralization would agree with the MREE enrichment observed in the water of Lake Kinneret. At the same time, the fertilization of the lake water from Fe disposal, provides the biomass growth that influences the micrograzer excretion [*Li et al*., 2014] and leads to the increase of the organic load in the lake. Although oxidizing conditions occur in shallow water layer (Eh = 0.19 V), the latter conditions contribute to maintain both Ce(III) and Ce(IV) in the dissolved phase [*Pourret et al*., 2008; *Censi et al*., 2010; *Loges et al*., 2012; *Kraemer et al*., 2017], probably associated to the colloidal fraction occurring therein. As a consequence, the Ce anomaly, typical of oxidizing water systems is poorly developed or does not occur.

Against the MREE enrichment shown by shale-normalized patterns of Group-1 waters, Group-2 waters are characterized by positive Eu anomalies (Figure 6). This difference is hard to explain according to the amplitude of rock-water interactions since both the studied group waters flow through the same rock types: Upper Cretaceous limestones from the Judea Group, arenaceous sediments from the Dead Sea Group and limestone debris and sands from the Arava Graben [*Möller et al*., 2003]. Moreover, all these lithotypes have very similar REE distribution [*Möller et al*., 2003]. As a consequence, the hypothesis that the different REE features observed in Group-1 and Group-2 waters can be simply related to rock-water interactions can be ruled out. Against this background, the different REE behavior recognized in Group-1 and Group-2 waters can be determined by redox conditions, as suggested by the different Ce and Eu behavior in the two water groups (Figure 9).

Ce and Eu are redox sensitive elements, with two oxidation states. Ce can occur as Ce^{3+} and Ce^{4+} whereas Eu has 2+ and 3+ oxidation states. In the studied samples, Ce and Eu anomalies cover a wide range of values from 0.3 to 0.97 and from 1.09 to 6.29, respectively. Figure 9 shows different distribution of Eu and Ce anomalies in Groups 1 and 2 according to their different redox conditions. Positive Eh value-Group-1 waters show almost always negative Ce anomalies ($Ce/Ce^{*} < 0.95$; see *Bau and Dulski* [1996] for a detailed discussion) coupled with slight positive Eu anomaly values ($1.1 \leq Eu/Eu^{*} \leq 1.3$). Negative Eh values-Group-2 waters show slightly negative or absent Ce anomalies coupled to stronger positive Eu anomalies up to 6.29. These features suggest that in Group-1 waters Ce and Eu occur in the respective oxidized forms in agreement with the limited extent of Eu anomaly and the Ce scavenging as CeO_2 under oxidizing conditions

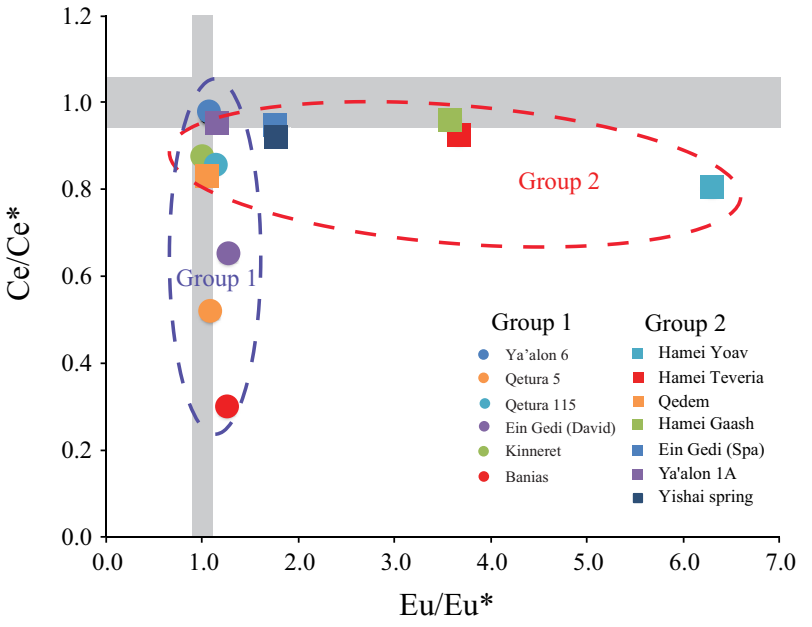

Figure 9. Relationship between Eu anomalies and Ce anomalies. The grey bands indicate negligible Ce/Ce* and Eu/Eu* values related to analytical precision (see *Bau and Dulski* [1996] for a detailed discussion). Standard errors are within the symbols.

onto Fe-oxyhydroxides [*Koschinsky and Hein*, 2003; *Seto and Akagi*, 2008]. On the contrary, Ce and Eu could occur as reduced Ce^{3+} and Eu^{2+} aqueous species in Group-2 waters, as suggested the limited extent of Ce anomalies and by evidences of model calculations showing the Eu occurrence as Eu^{2+}. The latter suggestion could explain the observed positive Eu anomalies in Group-2 waters due the larger Eu^{2+} stability in aqueous phase relative to its trivalent neighbors Sm^{3+} and Gd^{3+} [*Bau*, 1991; *Bau and Moller*, 1993].

6. Conclusions

The study of Zr, Hf, and REE distributions in thermal and natural waters spanning a wide range of physical-chemical and salt content conditions shows a strong dependence of Zr/Hf, Eu/Eu*, and Ce/Ce* on Eh values. The latter parameter allows to group the studied waters according to their oversaturation relative to Fe-oxyhydroxides ($Eh > -0.1$ V) and pyrite ($Eh < -0.25$ V), respectively. The deposition of Fe-oxyhydroxides suggested by geochemical modeling involves Hf fractionation relative to Zr onto solid surfaces influencing the dissolved Zr/Hf signature. At the same time, the redox conditions are responsible of the aqueous Eu speciation as Eu^{2+} according to $Eh < -0.25$ V. The latter process enhances the dissolved Eu stability relative to their neighbors along the REE series and the presence of positive Eu anomalies in these waters. Analogously, the oxidative Ce scavenging as CeO_2 onto surfaces of Fe-oxyhydroxides allows negative Ce anomaly values in oxidizing waters. A very interesting point of this study is that the dissolved REE speciation cannot simply explain the observed distribution in natural waters and the solid-liquid processes play a key role on the geochemical behavior of these elements.

Acknowledgments
We are indebted with Ittai Gavrieli, Ludwik Halicz, and Yehudit Harlavan for their assistance and cooperation during sample collection and preliminary lab treatment of collected waters. We thank the Istituto Nazionale di Geofisica e Vulcanologia—Palermo (INGV) for the analytical support. This paper benefited from the reviews and comments of I. Gavrieli. We are also indebted with Matthew I. Leybourne for the critical review of the early version of the manuscript. This paper reports scientific results belonging to the PhD project of Claudio Inguaggiato. This research was partially funded by the contract CORI 2012 and the PJAUTF005478 fund (University of Palermo). Supporting data are included as tables in the supporting information.

References

Aja, S. U., S. A. Wood, and A. E. WilliamsJones (1995), The aqueous geochemistry of Zr and the solubility of some Zr-bearing minerals, *Appl. Geochem.*, *10*(6), 603–620.

Bach, W., S. Roberts, D. A. Vanko, R. A. Binns, C. J. Yeats, P. R. Craddock, and S. E. Humphris (2003), Controls of fluid chemistry and complexation on rare-earth element contents of anhydrite from the Pacmanus subseafloor hydrothermal system, Manus Basin, Papua New Guinea, *Miner. Deposita*, *38*(8), 916–935.

Bau, M. (1991), Rare-earth element mobility during hydrothermal and metamorphic fluid-rock interaction and the significance of the oxidation state of europium, *Chem. Geol.*, *93*(3-4), 219–230.

Bau, M. (1996), Controls on the fractionation of isovalent trace elements in magmatic and aqueous systems: Evidence from Y/Ho, Zr/Hf, and lanthanide tetrad effect, *Contrib. Mineral. Petrol.*, *123*(3), 323–333.

Bau, M. (1999), Scavenging of dissolved yttrium and rare earths by precipitating iron oxyhydroxide: Experimental evidence for Ce oxidation, Y-Ho fractionation, and lanthanide tetrad effect, *Geochim. Cosmochim. Acta*, *63*(1), 67–77.

Bau, M., and P. Dulski (1995), Comparative study of yttrium and rare-earth element behaviours in fluorine-rich hydrothermal fluids, *Contrib. Mineral. Petrol.*, *119*(2-3), 213–223.
Bau, M., and P. Dulski (1996), Distribution of yttrium and rare-earth elements in the Penge and Kuruman iron-formations, Transvaal Supergroup, South Africa, *Precambrian Res.*, *79*(1-2), 37–55.
Bau, M., and P. Dulski (1999), Comparing yttrium and rare earths in hydrothermal fluids from the Mid-Atlantic Ridge: Implications for Y and REE behaviour during near-vent mixing and for the Y/Ho ratio of proterozoic seawater, *Chem. Geol.*, *155*(1-2), 77–90.
Bau, M., and A. Koschinsky (2006), Hafnium and neodymium isotopes in seawater and in ferromanganese crusts: The "element perspective", *Earth Planet. Sci. Lett.*, *241*(3-4), 952–961.
Bau, M., and P. Moller (1993), Rare-earth element systematics of the chemically precipitated component in early Precambrian iron formations and the evolution of the terrestrial atmosphere-hydrosphere-lithosphere system, *Geochim. Cosmochim. Acta*, *57*(10), 2239–2249.
Bau, M., A. Usui, B. Pracejus, N. Mita, Y. Kanai, W. Irber, and P. Dulski (1998), Geochemistry of low-temperature water-rock interaction: Evidence from natural waters, andesite, and iron-oxyhydroxide precipitates at Nishiki-numa iron-spring, Hokkaido, Japan, *Chem. Geol.*, *151*(1-4), 293–307.
Biddau, R., M. Bensimon, R. Cidu, and A. Parriaux (2009), Rare earth elements in groundwater from different Alpine aquifers, *Chem. Erde Geochem.*, *69*(4), 327–339.
Bulbul, M.S., C. Kantar, and S. Keskin (2016), Role of major groundwater ions on reductive Cr[VI] immobilization in subsurface systems with pyrite, Water Air Soil Pollut., 227, 1–11.
Byrne, R. H. (2002), Inorganic speciation of dissolved elements in seawater: The influence of pH on concentration ratios, *Geochem. Trans.*, *3*, 11–16.
Byrne, R. H., and E. R. Sholkovitz (1996), Chapter 158 Marine chemistry and geochemistry of the lanthanides, in *Handbook on the Physics and Chemistry of Rare Earths*, edited by K. A. Gschneidner, Jr. and L. Eyring, vol. 23, pp. 497–593, Elsevier Science.
Censi, P., P. Comin-Chiaramonti, G. Demarchi, A. Longinelli, and D. Orue (1989), Geochemistry and CO isotopes of the Chiriguelo carbonatite, northeastern Paraguay, *J. South Am. Earth Sci.*, *2*(3), 295–303.
Censi, P., M. Sprovieri, D. Larocca, P. Aricò, F. Saiano, S. Mazzola, and P. Ferla (2007a), Alteration effects of volcanic ash in seawater: Anomalous Y/Ho ratios in coastal waters of the Central Mediterranean Sea, *Geochim. Cosmochim. Acta*, *71*(22), 5405–5422.
Censi, P., M. Sprovieri, F. Saiano, S. I. Di Geronimo, D. Larocca, and F. Placenti (2007b), The behaviour of REEs in Thailand's Mae Klong estuary: Suggestions from the Y/Ho ratios and lanthanide tetrad effects, *Estuarine Coastal Shelf Sci.*, *71*(3-4), 569–579.
Censi, P., P. Zuddas, L. A. Randazzo, F. Saiano, S. Mazzola, P. Aricò, A. Cuttitta, and R. Punturo (2010), Influence of dissolved organic matter on rare earth elements and yttrium distributions in coastal waters, *Chem. Ecol.*, *26*(2), 123–135.
Censi, P., F. Saiano, P. Zuddas, A. Nicosia, S. Mazzola, and M. Raso (2014), Authigenic phase formation and microbial activity control Zr, Hf, and rare earth element distributions in deep-sea brine sediments, *Biogeosciences*, *11*(4), 1125–1136.
Censi, P., M. Cangemi, L. Brusca, P. Madonia, F. Saiano, and P. Zuddas (2015), The behavior of rare-earth elements, Zr and Hf during biologically-mediated deposition of silica-stromatolites and carbonate-rich microbial mats, *Gondwana Res.*, *27*, 209–2015.
Comin-Chiaramonti, P., A. Cundari, C. B. Gomes, E. M. Piccirillo, P. Censi, A. DeMin, G. Bellieni, V. F. Velazquez, and D. Orué (1992), Potassic dyke swarm in the Sapucai Graben, eastern Paraguay: Petrographical, mineralogical and geochemical outlines, *Lithos*, *28*(3-6), 283–301.
Comin-Chiaramonti, P., C. De Barros Gomes, A. Cundari, F. Castorina, and P. Censi (2007), A review of carbonatitic magmatism in the Paraná-Angola-Namibia (PAN) system, *Period. Mineral.*, *76*(3), 25–78.
Firdaus, M. L., K. Norisuye, T. Sato, S. Urushihara, Y. Nakagawa, S. Umetani, and Y. Sohrin (2007), Preconcentration of Zr, Hf, Nb, Ta and W in seawater using solid-phase extraction on TSK-8-hydroxyquinoline resin and determination by inductively coupled plasma-mass spectrometry, *Anal. Chim. Acta*, *583*(2), 296–302.
Firdaus, M. L., T. Minami, K. Norisuye, and Y. Sohrin (2011), Strong elemental fractionation of Zr-Hf and Nb-Ta across the Pacific Ocean, *Nat. Geosci.*, *4*(4), 227–230.
Frank, M. (2011), Oceanography: Chemical twins, separated, *Nat. Geosci.*, *4*(4), 220–221.
Garfunkel, Z. (1981), Internal structure of the Dead Sea leaky transform (rift) in relation to plate kinematics, *Tectonophysics*, *80*(1-4), 81–108.
Ginzburg, A., and G. Gvirtzman (1979), Changes in the crust and in the sedimentary cover across the transition from the Arabian Platform to the Mediterranean Basin: Evidence from seismic refraction and sedimentary studies in Israel and in Sinai, *Sediment. Geol.*, *23*(1-4), 19–36.
Göb, S., A. Loges, N. Nolde, M. Bau, D. E. Jacob, and G. Markl (2013), Major and trace element compositions (including REE) of mineral, thermal, mine and surface waters in SW Germany and implications for water-rock interaction, *Appl. Geochem.*, *33*, 127–152.
Godfrey, L. V., W. M. White, and V. J. M. Salters (1996), Dissolved zirconium and hafnium distributions across a shelf break in the northeastern Atlantic Ocean, *Geochim. Cosmochim. Acta*, *60*(21), 3995–4006.
Godfrey, L. V., B. Zimmermann, D. C. Lee, R. L. King, J. D. Vervoort, R. M. Sherrell, and A. N. Halliday (2009), Hafnium and neodymium isotope variations in NE Atlantic seawater, *Geochem. Geophys. Geosyst.*, *10*, Q08015, doi:10.1029/2009GC002508.
Greitzer, Y., and D. Levitte (2000), Geothermal update report from Israel 1999, paper presented at World Geothermal Congress 2000 Kyushu - Tohoku, Japan, May 28 - June 10, 2000.
Gur, D., M. Bar-Matthews, and E. Sass (2003), Hydrochemistry of the main Jordan River sources: Dan, Banias, and Kezinim springs, north Hula Valley, Israel, *Isr. J. Earth Sci.*, *52*(3-4), 155–178.
Hannigan, R. E., and E. R. Sholkovitz (2001), The development of middle rare earth element enrichments in freshwaters: Weathering of phosphate minerals, *Chem. Geol.*, *175*(3-4), 495–508.
Inguaggiato, C., P. Censi, P. Zuddas, J. M. Londono, Z. Chacon, D. Alzate, L. Brusca, and W. D'Alessandro (2015), Geochemistry of REE, Zr and Hf in a wide range of pH and water composition: The Nevado del Ruiz volcano-hydrothermal system (Colombia), *Chem. Geol.*, *417*, 125–133.
Inguaggiato, C., P. Censi, W. D'Alessandro, and P. Zuddas (2016a), Geochemical characterisation of gases along the dead sea rift: Evidences of mantle-CO_2 degassing, *J. Volcanol. Geotherm. Res.*, *320*, 50–57.
Inguaggiato, C., P. Censi, P. Zuddas, W. D'Alessandro, L. Brusca, G. Pecoraino, and S. Bellomo (2016b), Zirconium-hafnium and rare earth element signatures discriminating the effect of atmospheric fallout from hydrothermal input in volcanic lake water, *Chem. Geol.*, *433*, 1–11.
Jochum, K. P., H. M. Seufert, B. Spettel, and H. Palme (1986), The solar-system abundances of Nb, Ta, and Y, and the relative abundances of refractory lithophile elements in differentiated planetary bodies, *Geochim. Cosmochim. Acta*, *50*(6), 1173–1183.
Johannesson, K. H., J. Tang, J. M. Daniels, W. J. Bounds, and D. J. Burdige (2004), Rare earth element concentrations and speciation in organic-rich blackwaters of the Great Dismal Swamp, Virginia, USA, *Chem. Geol.*, *209*(3-4), 271–294.
Klungness, G. D., and R. H. Byrne (2000), Comparative hydrolysis behavior of the rare earths and yttrium: The influence of temperature and ionic strength, *Polyhedron*, *19*(1), 99–107.

Koschinsky, A., and J. R. Hein (2003), Uptake of elements from seawater by ferromanganese crusts: solid-phase associations and seawater speciation, *Mar. Geol.*, *198*(3-4), 331–351.
Kraemer, D., N. Tepe, O. Pourret, and M. Bau (2017), Negative cerium anomalies in manganese (hydr)oxide precipitates due to cerium oxidation in the presence of dissolved siderophores, *Geochim. Cosmochim. Acta*, *196*, 197–208.
Lee, J. H., and R. H. Byrne (1992), Examination of comparative rare-earth element complexation behavior using linear free-energy relationships, *Geochim. Cosmochim. Acta*, *56*(3), 1127–1137.
Levitte, D., and Y. Greitzer (2005), Geothermal update report for Israel 2005, in Proceedings World Geothermal Congress 2005 Antalya, Turkey, 24-29 April 2005.
Leybourne, M. I., J. M. Peter, D. Layton-Matthews, J. Volesky, and D. R. Boyle (2006), Mobility and fractionation of rare earth elements during supergene weathering and gossan formation and chemical modification of massive sulfide gossan, *Geochim. Cosmochim. Acta*, *70*(5), 1097–1112.
Li, Y., G. Gal, V. Makler-Pick, A. M. Waite, L. C. Bruce, and M. R. Hipsey (2014), Examination of the role of the microbial loop in regulating lake nutrient stoichiometry and phytoplankton dynamics, *Biogeosciences*, *11*(11), 2939–2960.
Loges, A., T. Wagner, M. Barth, M. Bau, S. Göb, and G. Markl (2012), Negative Ce anomalies in Mn oxides: The role of Ce 4+ mobility during water-mineral interaction, *Geochim. Cosmochim. Acta*, *86*, 296–317.
Luo, Y. R., and R. H. Byrne (2000), The ionic strength dependence of rare earth and yttrium fluoride complexation at 25°C, *J. Solution Chem.*, *29*(11), 1089–1099.
Luo, Y. R., and R. H. Byrne (2001), Yttrium and rare Earth element complexation by chloride ions at 25°C, *J. Solution Chem.*, *30*(9), 837–845.
Luo, Y. R., and R. H. Byrne (2004), Carbonate complexation of yttrium and the rare earth elements in natural waters, *Geochim. Cosmochim. Acta*, *68*(4), 691–699.
Lustrino, M., and M. Wilson (2007), The circum-Mediterranean anorogenic Cenozoic igneous province, *Earth Sci. Rev.*, *81*(1-2), 1–65.
Lutfi Firdaus, M., K. Norisuye, Y. Nakagawa, S. Nakatsuka, and Y. Sohrin (2008), Dissolved and labile particulate Zr, Hf, Nb, Ta, Mo and W in the western North Pacific Ocean, *J. Oceanogr.*, *64*(2), 247–257.
Marsac, R., S. Martin, J. F. Boily, and K. Hanna (2016), Oxolinic acid binding at goethite and akaganéite surfaces: Experimental study and modeling, *Environ. Sci. Technol.*, *50*(2), 660–668.
Mckelvey, B. A., and K. J. Orians (1993), Dissolved zirconium in the North Pacific-Ocean, *Geochim. Cosmochim. Acta*, *57*(15), 3801–3805.
McKelvey, B. A., and K. J. Orians (1998), The determination of dissolved zirconium and hafnium from seawater using isotope dilution inductively coupled plasma mass spectrometry, *Mar. Chem.*, *60*(3-4), 245–255.
Mechie, J., Z. Ben-Avraham, M. H. Weber, H. J. Götze, I. Koulakov, A. Mohsen, and M. Stiller (2013), The distribution of Moho depths beneath the Arabian plate and margins, *Tectonophysics*, *609*, 234–249.
Millero, F. J. (1992), Stability-constants for the formation of rare-earth inorganic complexes as a function of ionic-strength, *Geochim. Cosmochim. Acta*, *56*(8), 3123–3132.
Möller, P., E. Rosenthal, P. Dulski, S. Geyer, and Y. Guttman (2003), Rare earths and yttrium hydrostratigraphy along the Lake Kinneret-Dead Sea-Arava transform fault, Israel and adjoining territories, *Appl. Geochem.*, *18*(10), 1613–1628.
Moller, P., E. Rosenthal, S. Geyer, J. Guttman, P. Dulski, M. Rybakov, M. Zilberbrand, C. Jahnke, and A. Flexer (2007), Hydrochemical processes in the lower Jordan valley and in the Dead Sea area, *Chem. Geol.*, *239*(1-2), 27–49.
Möller, P., E. Rosenthal, and S. Geyer (2009), Regional hydrochemical and hydrogeological aspects of groundwater in the Jordan-Dead Sea Rift system, in *The Water of the Jordan Valley: Scarcity and Deterioration of Groundwater and its Impact on the Regional Development*, edited by P. Moller and E. Rosenthal, pp. 149–180, Springer-Verlag Berlin Heidelberg.
Ohta, A., H. Kagi, M. Nomura, H. Shitsuno, and I. Kawabe (2009), Coordination study of rare earth elements on Fe oxyhydroxide and Mn dioxides: Part ii. Correspondence of structural change to irregular variations of partitioning coeffcients and tetrad effect variations appearing in interatomic distances, *Am. Mineral.*, *94*(4), 476–486.
Parkhurst, D. L., and C. A. J. Appelo (2010), User's Guide to PHREEQC *(Version 2.17.5)—A Computer program for Speciation, Batch-Reaction, One-Dimensional Transport and Inverse Geochemical Calculations*. U.S. Department of the Interior/ U.S. Geological Survey. Denver. Colorado, 2010. [Available at http://www.brr.cr.usgs.gov/projects/GWC_coupled/phreeqc/index.html.]
Pershina, V., D. Trubert, C. Le Naour, and J. V. Kratz (2002), Theoretical predictions of hydrolysis and complex formation of group-4 elements Zr, Hf and Rf in HF and HCl solutions, *Radiochim. Acta*, *90*(12), 869–877.
Playa, E., D. I. Cendon, A. Trave, A. R. Chivas, and A. Garcia (2007), Non-marine evaporites with both inherited marine and continental signatures: The Gulf of Carpentaria, Australia, at similar to 70 ka, *Sediment. Geol.*, *201*(3-4), 267–285.
Pourret, O., M. Davranche, G. Gruau, and A. Dia (2008), New insights into cerium anomalies in organic-rich alkaline waters, *Chem. Geol.*, *251*(1-4), 120–127.
Qu, C., G. Liu, and Y. Zhao (2009), Experimental study on the fractionation of yttrium from holmium during the coprecipitation with calcium carbonates in seawater solutions, *Geochem. J.*, *43*(6), 403–414.
Raso, M., P. Censi, and F. Saiano (2013), Simultaneous determinations of zirconium, hafnium, yttrium and lanthanides in seawater according to a co-precipitation technique onto iron-hydroxide, *Talanta*, *116*, 1085–1090.
Reznikov, M., Z. Ben-Avraham, Z. Garfunkel, H. Gvirtzman, and Y. Rotstein (2004), Structural and stratigraphic framework of Lake Kinneret, *Isr. J. Earth Sci.*, *53*(3-4), 131–149.
Ruberti, E., F. Castorina, P. Censi, P. Comin-Chiaramonti, C. B. Gomes, P. Antonini, and F. R. D. Andrade (2002), The geochemistry of the Barra do Itapirapu√£carbonatite (Ponta Grossa Arch, Brazil): A multiple stockwork, *J. South Am. Earth Sci.*, *15*(2), 215–228.
Rybakov, M., and A. Segev (2004), Top of the crystalline basement in the Levant, *Geochem. Geophys. Geosyst.*, *5*, Q09001, doi:10.1029/2004GC000690.
Schijf, J., and R. H. Byrne (2004), Determination of <inf>SO4β1</inf> for yttrium and the rare earth elements at I = 0.66 m and t = 25°C-implications for YREE solution speciation in sulfate-rich waters, Geochim. Cosmochim. Acta, 68(13), 2825-2837.
Schmidt, K., M. Bau, J. R. Hein, and A. Koschinsky (2014), Fractionation of the geochemical twins Zr-Hf and Nb-Ta during scavenging from seawater by hydrogenetic ferromanganese crusts, *Geochim. Cosmochim. Acta*, *140*, 468–487.
Seto, M., and T. Akagi (2008), Chemical condition for the appearance of a negative Ce anomaly in stream waters and groundwaters, *Geochem. J.*, *42*(4), 371–380.
Shaked, Y., Y. Erel, and A. Sukenik (2002), Phytoplankton-mediated redox cycle of iron in the epilimnion of Lake Kinneret, *Environ. Sci. Technol.*, *36*(3), 460–467.
Shaw, T. J., T. Duncan, and B. Schnetger (2003), A preconcentration/matrix reduction method for the analysis of rare earth elements in seawater and groundwaters by isotope dilution ICPMS, *Anal. Chem.*, *75*(14), 3396–3403.
Sholkovitz, E. R. (1995), The aquatic chemistry of rare earth elements in rivers and estuaries, *Aquat. Geochem.*, *1*(1), 1–34.

Siebert, C., E. Rosenthal, P. Möller, T. Rödiger, and M. Meiler (2012), The hydrochemical identification of groundwater flowing to the Bet She'an-Harod multiaquifer system (Lower Jordan Valley) by rare earth elements, yttrium, stable isotopes (H, O) and Tritium, *Appl. Geochem.*, *27*(3), 703–714.

Sneh, A., Y. Bartov, T. Weissbrod, and M. Rosensaft (1998), Geological map of Israel, sheet 4, scale 1:200000, Geol. Surv. Isr., Jerusalem.

Sverjensky, D. A. (1984), Europium redox equilibria in aqueous solution, *Earth Planet. Sci. Lett.*, *67*, 70–78.

Takahashi, Y., H. Yoshida, N. Sato, K. Hama, Y. Yusa, and H. Shimizu (2002), W- and M-type tetrad effects in REE patterns for water-rock systems in the Tono uranium deposit, central Japan, *Chem. Geol.*, *184*(3-4), 311–335.

Tanaka, K., A. Ohta, and I. Kawabe (2004), Experimental REE partitioning between calcite and aqueous solution at 25°C and 1 atm: Constraints on the incorporation of seawater REE into semount-type limestones, *Geochem. J.*, *38*(1), 19–32.

Tanaka, K., Y. Takahashi, and H. Shimizu (2008), Local structure of Y and Ho in calcite and its relevance to Y fractionation from Ho in partitioning between calcite and aqueous solution, *Chem. Geol.*, *248*(1-2), 104–113.

Tang, J., and K. H. Johannesson (2006), Controls on the geochemistry of rare earth elements along a groundwater flow path in the Carrizo Sand aquifer, Texas, USA, *Chem. Geol.*, *225*(1-2), 156–171.

Taylor, S. R., and S. M. McLennan (1995), The geochemical evolution of the continental crust, *Rev. Geophys.*, *33*(2), 241–265.

Thiagarajan, N., and C. T. A. Lee (2004), Trace-element evidence for the origin of desert varnish by direct aqueous atmospheric deposition, *Earth Planet. Sci. Lett.*, *224*(1-2), 131–141.

Toulkeridis, T., P. Podwojewski, and N. Clauer (1998), Tracing the source of gypsum in New Caledonian soils by REE contents and S-Sr isotopic compositions, *Chem. Geol.*, *145*(1-2), 61–71.

Varekamp, J. C. (2015), The chemical composition and evolution of volcanic lakes, in *Volcanic Lakes*, edited by D. Rouwet, B. Christenson, F. Tassi, J. Vandemeulebrouck, pp. 93–123, Springer-Verlag Berlin Heidelberg.

Vergouw, J. M., A. Difeo, Z. Xu, and J. A. Finch (1998), An agglomeration study of sulphide minerals using zeta potential and settling rate. Part II: Sphalerite/pyrite and sphalerite/galena, *Miner. Eng.*, *11*(7), 605–614.

Weinstein, R., N. Paldor, D. A. Anati, and A. Hecht (2000), Internal seiches in the strongly stratified Dead Sea, *Isr. J. Earth Sci.*, *49*(1), 45–53.

Willie, S. N., and R. E. Sturgeon (2001), Determination of transition and rare earth elements in seawater by flow injection inductively coupled plasma time-of-flight mass spectrometry, *Spectrochim. Acta, Part B*, *56*(9), 1707–1716.

Wood, S. A. (2003), The geochemistry of rare earth elements and yttrium in geothermal waters, *Soc. Econ. Geol. Spec. Publ.*, *10*, 133–158.

Zak, I. (1967), *The Geology of Mt. Seom* [in Hebrew with English abstract], Hebrew Univ., Jerusalem.

Zhu, Y., T. Umemura, H. Haraguchi, K. Inagaki, and K. Chiba (2009), Determination of REEs in seawater by ICP-MS after on-line preconcentration using a syringe-driven chelating column, *Talanta*, *78*(3), 891–895.